COMPARATIVE STUDY OF SYMMETRIC AND ASYMMETRIC DEFORMATION OF AL SINGLE CRYSTAL UNDER MICRO SCALE LASER SHOCK PEENING

Paper M604

Sinisa Vukelic, Youneng Wang, Jeffrey W. Kysar, and Y. Lawrence Yao
Department of Mechanical Engineering, Columbia University, New York, NY 10027, United States

Abstract

Laser shock peening by a micron sized laser beam is a process in which compressive residual stresses are induced in order to improve material fatigue life of micro scale components. The size of the laser target interaction zone is of the same order of magnitude as the target material grains and thus the effects of anisotropic material response must be taken into account. Single crystals are therefore chosen to study such anisotropy. It is also of interest to investigate the response of symmetric and asymmetric slip systems with respect to the yield surface. In presented work, analytic, numerical and experimental investigations of two different orientations, (110) and $(1\,\bar{1}\,4)$ of aluminum single crystals are studied. Anisotropic slip line theory is employed for the construction of slip line fields for both orientations and compared with numerical results. Theory is further used to explain the difference in plastic deformation for two different orientations. Lattice rotations on the top surface and cross section are also measured using Electron Backscatter Diffraction (EBSD), while residual stress is measured using X-ray microdiffraction. Both the analytical and numerical models are then validated via experimental results.

1. Introduction

It is well known that process of shot peening is beneficial for improvement of fatigue behavior of treated parts. The process consists of bombarding of surface layer with hard particles which induce compressive stresses by repeated impacts. Laser shock peening (LSP) as a process was introduced in a second half of the twentieth century [7], [8], [9]. This is a surface treatment wherein laser induced shocks introduce compressive residual stress of the same order of magnitude as conventional shoot peening, but much deeper into the material resulting in the improvement of performance under cyclic loading of various materials, such as copper, aluminum, nickel etc. [13]. Also LSP is much easier to control than conventional shoot peening allowing treatment of only selected regions by precisely determining position of the laser. Another benefit is that LSP induces little or no change to surface finish. However, this technique has not been widely used in industry because of the expense of high power lasers needed to induce beam spot size of order of millimeters necessary in order to treat large areas.

In recent times, development of MEMS (micro electromechanical systems) raised the issue of improvement of reliability of components of those systems by using micro scale LSP (μLSP). In particular, μLSP can improve fatigue life and wear resistance of those components by altering residual stress distribution with a spatial resolution of several microns. In this process, the specimen is coated with aluminum foil or black paint so that the material to be treated is not subjected to high temperatures. Thus, residual stress is induced only by shock pressure and the process is considered as primarily mechanical; thus there is no microstructure change due elevated temperatures. Much work in this field has been performed on polycrystalline materials [27]. However, in μLSP the beam spot size is approximately several microns and the average grain size in polycrystalline aluminum and copper is about same of order of magnitude, which means that in most cases only a few grains at most are affected by a single laser pulse. Therefore the material properties must be considered as anisotropic and heterogeneous. This has motivated the study of single crystal aluminum and copper under laser shock processing in order to better understand the response due to anisotropy [5]. Residual stresses were measured using x-ray microdiffraction and the method introduced by Ungar [25] was used for calculation. A numerical model was established and the results compared to experiment for two different orientations of aluminum and copper single crystals, but without detailed exploration of single crystal plasticity.

The effect of the anisotropic material properties has also been studied analytically using anisotropic slip line theory. Slip line theory, originally founded by Prandtl [22] and Hencky [21] for isotropic materials was extended for the case of an elliptic yield surface by Hill [14] who also examined indentation by flat rigid die. Rice [23] further generalized the theory for materials of arbitrary anisotropy. Rice [24] also analyzed the stress distribution near crack tip fields

and introduced asymptotic crack tip stress field solutions for ideally plastic single crystal. Based on this work Crone et. al. [3] studied orientation dependence of plastic slip near notches. Slip line patterns related to various sets of orientations are analyzed both, analytically and numerically. Kysar et al. [19] employed this theory to find analytical solution for the stress distribution around a cylindrical void in a single crystal.

In order to predict stress distribution and plastic deformation size during μLSP anisotropic slip line theory is employed by Wang et al. [26] laser shock peening on an aluminum single crystal of $(1\bar{1}4)$ orientation. Non-symmetric orientation produces a single slip case which further enables derivation of unique close form solution. Gaussian pressure loading is approximated and an approximate analytical solution has been obtained which is further justified with numerical analysis. However, although it gives us some insight into material behavior, analysis of Al single crystal of $(1\bar{1}4)$ orientation is limited because this is a particular case in which only one slip system is active under the punch. Therefore it is of interest to investigate the more general double slip case in which two slip systems are active under the Gaussian pressure distribution. The (110) orientation is chosen because symmetry of yield surface simplifies the derivation and makes an analytical solution possible. Another motivation for work presented here is the fact that real applications will involve polycrystalline material in which orientation of grains has predominantly low Miller indices. Thus, the objective of this work is a comparative study of aluminum single crystal behavior under Gaussian pressure distribution induced by μLSP for two different orientations, one non-symmetric with high Miller index $(1\bar{1}4)$ and other symmetric with low Miller index (110). The deformation state will be characterized experimentally and anisotropic slip line theory will be used for derivation of stress distribution and deformation state induced by laser shock peening of single crystal surface under plane strain conditions. In addition, finite element method (FEM) simulation will be used for detailed analysis of single crystal plasticity as another perspective of study.

2. Laser Shock Processing

Under the radiation of an intense laser pulse a surface layer of a metal is instantaneously evaporated into plasma, characterized by high pressure (1~10 GPa) and high temperature. As the plasma expands, shock waves propagate into the target. Also it should be noted that there is significant difference in magnitude of the pressure depending whether the plasma is confined or not. If not confined, i.e. open air conditions, pressure can reach a peak value of only several tenths of one GPa. On the other hand, if confined by water or some other confining medium, Studies have shown [11] that shock pressure rises 5 times or more in comparison to the open air condition. Moreover, the duration of the shock pressure is 2 to 3 times longer than laser pulse itself. These pressures are far above the yield stress of most materials, thus it is very likely that plastic deformation will occur. In addition, if the peak shock pressure is above Hugoniot Elastic Limit (HEL) of the material of interest for sufficient time, there is a good chance that compressive residual stress distribution may be formed as a result of the plastic deformation [7].

For the case of laser shock processing, the target material is usually coated with metallic foil, paint or adhesives in order to prevent elevated temperatures from reaching the target. Thus, this process can be approximated as adiabatic, and therefore, only mechanical effects of pressure are taken into account in this analysis.

3. Experimental Setup

Because of its good mechanical and electrical properties, aluminum is widely used in various micro devices. For this study an aluminum single crystal is used. The sample is mounted on a three circle goniometer and its orientation is determined by Laue diffraction. The specimen is cut to size with wire electrical discharge machine (EDM) and the heat affected zone (HAZ) is removed with mechanical polishing. Finally, electro polishing is used in order to remove any material with residual stress. After gathering the required information from the surface, sample was sectioned along (100) direction with wire EDM and the cross section surface was again mechanically and electro polished in order to examine cross-section.

A frequency tripled Q-switched Nd:YAG laser with wavelength λ=355 nm in TEM_{00} mode is used for the μLSP experiments. Beam diameter is 12 μm, pulse duration is 50 ns and laser intensity is about 4 GW/cm^2. A thin polycrystalline aluminum foil is used as a coating and it is put tightly over evenly spread layer (10 μm thick) of grease. The specimen is put into a shallow container filled with distilled water which is about two millimeters above the sample's top surface as shown in Fig. 1. More details about laser shocking can be found at [27] and [5]. In order to obtain an approximate 2-D deformation, shocks are applied with 25 μm spacing in between along

[1$\bar{1}$0] direction as discussed in [5] and illustrated in Fig 2. Detailed discussion about formation of two dimensional deformation can be found in [24], [18] and [19]. Crone et al. [3] summarizes geometrical conditions that need to be met in order plane strain condition to take place.

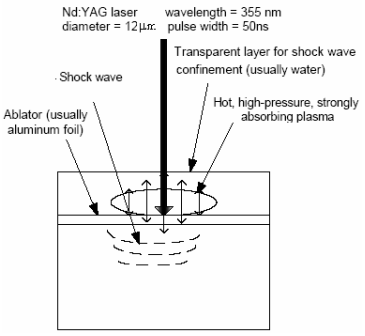

Figure 1: experimental setup

3.1 Electron Backscatter Diffraction

μLSP induces plastic deformation into the single crystal which can be determined experimentally by measuring lattice rotation in its deformed state [26], [18]. Lattice rotation is defined by Euler angles and the reference state is the known orientation of the crystal prior to shocking. Lattice rotation can be measured using Electron Backscatter Diffraction (EBSD) to measure crystallographic orientation as a function of spatial position.

In the work presented here, the treated surface is scanned via EBSD first, which provides information about lattice rotation on the treated surface. In order to get information about the depth of the affected region and magnitude of lattice rotation under the surface, EBSD mapping is employed on a cross section of the sample.

For these measurements a HKL Technology system attached to a JEOL JSM 5600LV scanning electron microscope was used. The scan area was 200 μm x 200 (μm) and 120 μm x 120 μm on surface and cross section, respectively, with 3 μm step size. Three Euler angles were acquired at each particular point in the automatic mode using external beam scanning.

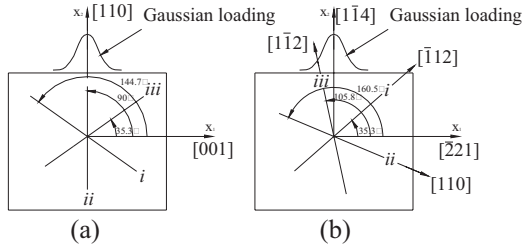

Figure 2: Plane strain slip systems corresponding to a) (110) orientation; b) (1$\bar{1}$4) orientation

3.2 X-ray Microdiffraction

Synchrotron radiation as a source of x-ray beams is used employed because of its high resolution and high intensity. Using glass capillary, the beam can be focused in such way that 1 μm spatial resolution can be achieved. Beamline X20A at the National Synchrotron Light Source at Brookhaven National Laboratory is used to measure residual stress. Monochromatic synchrotron radiation at 8.0 KeV is used. A Huber two-circle vertical diffractometer with partial chi (χ) and (ϕ) arcs is employed for diffraction. Measurement was conducted along a line perpendicular to the shock line with 10 μm spacing and acquired with modified version of SPEC software package. Data in form of X-ray profile obtained is further processed using Ungar's method [25]. More details about measurement technique can be found at [5].

4. Numerical Simulation Conditions of Single Crystals

Finite element analysis is performed based on single crystal plasticity theory by Asaro [1]. Background of this theory will be given in more detail in the following section. For the purpose of this analysis, a two dimensional model plane strain model is established. This is due the fact that deformation is two dimensional and material behaves similarly at any cross section along shock line. Simulation is quasi static, which although a gross oversimplification in comparison to highly dynamic character of μLSP, still gives a very good overview of process as a whole. Boundary conditions are specified as follows: at side edges there is no traction; vertical displacement at the bottom is zero and top surface experiences shock pressure loading. Loading distribution follows the Gaussian distribution:

$$P(x) = P_0 \exp\left(-\frac{x^2}{2R^2}\right) \qquad (1)$$

where R is beam radius, x is a distance from the center of Gaussian pressure distribution and P_o is peak pressure which is inserted into the model in non dimensional form P_0/τ_{CRSS} = 7. The analysis is simulated by commercial finite element methods (FEM) program ABAQUS/Standard which is combined with user defined subroutine UMAT, written by Huang [15] and modified by Kysar [17]. The aluminum slip systems are {111}<110>. Critical shear strength on each slip system is $\tau_{CRSS} \approx$ 1 MPa.

4.1. Single Crystal Micromechanics

According to [1], three operations can be distinct

during plastic deformation of a single crystal. Which when combined together determine the overall gradient F: first plastic slip through the undeformed crystal F^p, second rigid body rotation F^Ω, and finally combined lattice and material elastic deformation F^e. Therefore deformation gradient tensor can be written as:

$$F = F^e F^\Omega F^p \quad (2)$$

First two terms of equation can be combined together and general expression for deformation strain gradient becomes to: $F = F^* \cdot F^p$, where F^p is still deformation related to the plastic shear and F^* represents stretching and rotation of the crystal lattice. The velocity gradient, L, which is sum of spin rate tensor, Ω and deformation rate tensor, D can also be represented as $L = F \cdot F^{-1}$.Thus D and Ω can be decomposed into: $D = D^* + D^p$ and $\Omega = \Omega^* + \Omega^p$. In the absence of relative rotation of lattice and material or when only elastic deformation occurs, constitutive equation is:

$$\tau^\nabla = L : D - \sum_{\alpha=1}^{n} \left[L : P^{(\alpha)} + \beta^{(\alpha)} \right] \dot{\gamma}^{(\alpha)} \quad (3)$$

Where L is the tensor of elastic moduli, τ^∇ is Jaumann rate of Kirchoff stress tensor, $\beta^{(\alpha)} = W^{(\alpha)} \cdot \tau - \tau \cdot W^{(\alpha)}$ and $\dot{\gamma}^{(\alpha)}$ is shearing rate. Another important issue is the definition of Schmid stress, also known as resolved shear stress which is responsible for producing force on dislocations. From general expression of rate of working:

$$\tau : D^P = \sum_{\alpha=1}^{n} \tau : P^{(\alpha)} \dot{\gamma}^{(\alpha)} \quad (4)$$

we can find the Schmid stress on particular slip system α as:

$$\tau^{(\alpha)} = P^{(\alpha)} : \tau \quad (5)$$

5. Anisotropic Slip Line Theory

For better understanding of the deformation field development of an aluminum single crystal under μLSP, anisotropic slip line theory will be employed. Slip line theory was founded by Prandtl [21] and Hencky [22] for isotropic rigid-ideally plastic materials with circular yield surface under plane strain conditions. The effect of anisotropy was taken into account by Hill [14] who examined anisotropic rigid-ideally plastic materials with ellipsoidal yield surface. Further generalization was done by Booker and Davis [2] and Rice [23] employed principle of maximum plastic work to develop governing equations for material of an arbitrary anisotropy. Slip line theory treats incipient plane flow and it is assumed that plastic deformation occurs everywhere. After integration of equilibrium equations it is shown by [2] and [23] that:

$$\sigma - l = \text{constant along } \alpha\text{-lines}$$
$$\sigma + l = \text{constant along } \beta\text{-lines}$$

where l is the distance traversed in stress space. The solution has the surprisingly simple of two mutually orthogonal families of curves, denoted as α and β lines. In the case of single crystal plasticity, the α-lines correspond to slip directions **s**, and β-lines correspond to slip normals **n**.

Based on the slip line theory, pressure distribution solution for flat punch has first been derived by Hill [14] for anisotropic materials with elliptic yield surface and was solved with the generalized theory for arbitrary yield locus by Rice [23]. Wang et al. [26] employed anisotropic slip line theory to predict stress and deformation fields in case of laser shock peened single crystal. Using the fact that pressure in case of μLSP has a Gaussian spatial distribution [27], they assume that Gaussian pressure can be thought as a punch with non-uniform pressure distribution.

However, unlike flat punch, with constant pressure distributions it is not obvious where the punch 'ends' so the width of the punch in μLSP needs to be determined. In order to make good estimation of width, a derivation of pressure under which no plastic deformation occurs will be done first. The way to do that is to make an assumption of uniform pressure applied [26] and after that look for boundary value of pressure, P^*, at which plastic deformation is initiated.

Taking into consideration traction free boundary conditions at the surface $\sigma_{11} = 0$ and $\sigma_{12} = 0$ with uniform loading in vertical direction, $\sigma_{22} = -P^*$. Therefore with reference to Fig. 3 we can see that two slip systems will be activated under the punch when plastic deformation occurs. Using Schmid's law expressed as in [19]:

$$\sigma_{12} = \tan 2\phi_i \left(\frac{\sigma_{11} - \sigma_{22}}{2} \right) \pm \frac{\beta_i \tau_i}{\cos 2\phi_i} \quad (6)$$

where index *i* denotes active slip system, ϕ represents the angle between the slip system and $(\sigma_{11} - \sigma_{22})/2$ the abscissa of the stress coordinate system in Fig. 3 τ is critical resolved shear stress which can be experimentally determined and β is geometrical ratio, $\beta_1 = \beta_3 = 2/\sqrt{3}$ and, $\beta_2 = \sqrt{3}$ defined by Rice [24]. After imposing boundary conditions obtain the critical pressure at which plastic deformation initiates:

$$P^* = \mp \frac{2\beta_i \tau_i}{\sin 2\phi_i} \quad (7)$$

Once P^* is obtained, substituting P(x) with P^* in Gaussian pressure distribution yields:

$$P^* = P_0 \exp\left(-\frac{x^2}{2R^2}\right) \quad (8)$$

where R is radius of the plasma, and x is a distance form the center of the punch which needs to be determined. Value P^* is closely related to choice of orientation and its impact on determination of punch radius will be explained in next section. Equation 8 can be solved for x to find the approximate distance from the laser shock at which plastic deformation ceases.

6. Results and Discussion

6.1.1 Analytical Prediction of Slip Sectors for (110) and (1$\bar{1}$4) Orientations

The different crystallographic orientation of this study raises new questions that need to be addressed. In (110) case, orientation of a single crystal is such that corner of polygon which bounds yield surface is lies on the $(\sigma_{11} - \sigma_{22})/2$ axis which can be seen at Figure 3. The main difference between (1 $\bar{1}$ 4) orientation and (110) orientation is that in the latter case two slip systems have to be taken into account. Thus, details of both, stress and deformation field will be is influenced by the orientation.

Starting from Schmid's law in section 5 by applying boundary conditions, in general we get two different values of P^* for the slip systems i and iii:

$$\left(P^*\right)_1 = \mp \frac{2\beta_1 \tau_1}{\sin 2\phi_1} \quad (9)$$

$$\left(P^*\right)_3 = \mp \frac{2\beta_3 \tau_3}{\sin 2\phi_3} \quad (10)$$

For the (1$\bar{1}$4) orientation $(P^*)_1 < (P^*)_3$ so that only one slip system is active under the Gaussian pressure distribution. Figure 3b shows yield surface for (1$\bar{1}$4) orientation. On the other hand the absolute values of P^* are equal for both slip system i and iii for (110) which leads to double slip. This is due to the symmetry of yield locus such that:

$$\left|P^*\right|_1 = \left|P^*\right|_3 \quad (11)$$

$$\phi_1 = -\phi_3 \quad (12)$$

Therefore punch radius can also be estimated in case of (110) orientation. After P^* is determined from equation (7), an approximate punch radius can be derived as follows:

$$x_p = R\sqrt{\ln \frac{P_0^2 \sin^2 \phi}{(2\beta\tau)^2}} \quad (13)$$

This solution gives an order of magnitude value and actual value should be scaled $x_p' = c \cdot x_p$, where c is dimensionless constant determined from numerical simulation.

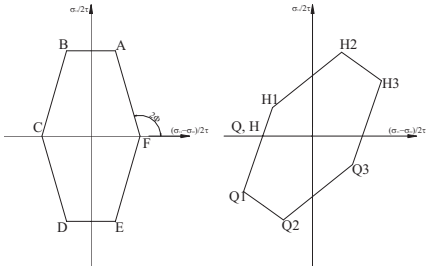

(a) (b)

Figure 3: Yield surface contour for a) (110) b) (1$\bar{1}$4) orientation

Once the approximate radius of the punch is calculated based on the geometry, center fan regions at both ends of Gaussian punch can be constructed from concepts of Rice [23], [24]. Slip line field for both, symmetric and asymmetric case can be seen in Figure 4. Regions within the centered fans correspond to the vertices on the yield contour. From Fig. 4 it can be seen that symmetric yield surface corresponds to symmetric slip line field and vice versa. It can also be seen that field is divided into sectors which represents areas of constant stress.

This arises from the assumption that material is rigid ideally plastic and there is no change in magnitude of stress in radial direction. Boundaries of these sectors are slip directions and slip normals which represent lines of discontinuity. More detailed discussion about stress discontinuity at slip lines and slip normals and conditions that need to be satisfied can be found in [24]. Figure 4 shows that beside two center fans there are three triangular regions, one region below the punch and two beyond. Rice [23] gave explanation why center fan exists at both ends of the punch. From Fig. 4a the geometry of the slip line field can also give us an estimate of the size of plastically deformed region for (110) and (1$\bar{1}$4) case, respectively:

$$L = 2x_P\left(1 + \frac{1}{\cos\left(\frac{\pi}{2} - \phi\right)\cos\phi}\right) = 2cR\sqrt{\ln\frac{P_o^2 \sin^2\phi}{(2\beta\tau)^2}}\left(1 + \frac{1}{\cos\left(\frac{\pi}{2} - \phi\right)\cos\phi}\right)$$

$$L = 2x_p\left(1 + \cot\phi + \tan\phi\right) = 2\sqrt{2}cR\sqrt{\ln\left(\frac{P_o}{2A}\right) + \ln\sin 2\phi}\left(1 + \cot\phi + \tan\phi\right) \quad (14)$$

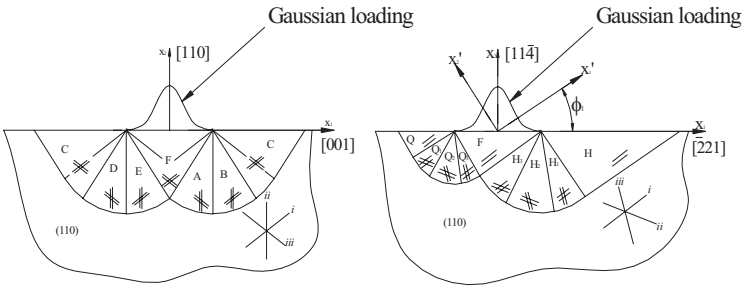

(a) (b)

Figure 4: Geometry of slip line field under Gaussian loading a) (110) orientation b) (1$\bar{1}$4) orientation

6.1.2. Analytical Prediction of Lattice Rotation for (110) and (1$\bar{1}$4) Orientations

As discussed previously in section 4.1. the spin tensor Ω consists of Ω^* which correspond to lattice rotation and Ω^P associated with plastic slip. Following [1] we can express plastic part of rate of spin Ω^P as:

$$\Omega^P = \sum_{\alpha=1}^{N} W^{(\alpha)} \cdot \dot{\gamma}^{(\alpha)} \tag{15}$$

where α represents active slip system, $\dot{\gamma}$ is rate of shear and tensor W is defined as:

$$W = \frac{1}{2}\left(s^{(\alpha)} n^{(\alpha)} - n^{(\alpha)} s^{(\alpha)}\right) \tag{16}$$

where **s** is unit vector in slip direction and **n** unit vector normal to slip plane.
Therefore Ω^* can be rewritten as:

$$\Omega^* = \Omega - \frac{1}{2}\sum_{i=1}^{N} \dot{\gamma}\left(s_i n_j - s_j n_i\right) \tag{17}$$

This equation gives us relation between spin tensor responsible for lattice rotation and slip rate of each active slip system. Therefore lattice rotation is directly related to the slip at each slip system. Taking into account the plane strain condition this can be expressed as:

$$\Omega^* = \Omega - \frac{1}{2}\sum_{i=1}^{N} \dot{\gamma}\left(S_i N_j - S_j N_i\right)\beta_i \tag{18}$$

Since $S_iN_i = 0$ is necessary condition for plain strain condition to occur [24] it follows that $S_1=N_2$, $S_2=-N_1$. So that term in parentheses reduces identically to unity. The only factor left under the summation is strain rate, which is different for each slip system.

Unlike the (1$\bar{1}$4) case where only one slip system is active, in the (110) orientation there are two active slip systems in the triangular regions. The contribution of each slip system to the lattice rotation can be seen through shear stress acting on particular slip system. Implementing anisotropic slip line theory for (110) case, it can be shown that the shear stress on each slip system has the same sign. This leads to conclusion that deformation associated with each slip adds to total deformation. Furthermore, (110) orientation is symmetric and therefore each active slip system equally contributes to magnitude of lattice deformation. On the other hand, in (1$\bar{1}$4) case we have only one active slip system and therefore rotation is expected to be less than that in symmetric case. More detailed discussion about numerical and experimental results is given below.

6.2. Numerical results

6.2.1. Slip Sectors and Shear Strain increments

According to the analytical solution, the entire deformation field is divided into sectors. In each of those sectors one or two slips are active. As discussed by Rice [24], boundaries of sectors are slip directions and slip normals which represent lines of stress discontinuity. The numerical model agrees well with analytical solution as shown by Wang et al. [26]. Here, emphasis will be put on comparison between symmetric and asymmetric orientation. Because of that it is of interest to closely examine shear strain increments for each slip system as well as total shear strain increment, which are shown on Figures 5a and 5b for both (110) and (1$\bar{1}$4) cases. From Figure 5a it can be seen, that in the (110) case, shear increments associated with slips i and iii are antisymmetric with respect to the plane which contains shock line and its perpendicular to the surface. Shear increment ii is symmetric with respect to same plane. Thus total shear increment is also symmetric. On the other hand in the (1$\bar{1}$4) (Fig. 5b) orientation at the right side of the model, with respect to the plane defined above, magnitude and distribution of increments $\gamma^{(1)}$, $\gamma^{(2)}$, $\gamma^{(3)}$, as well as total shear increment $\gamma^{(tot)}$ are much larger, than on the left side as seen on the Figure 5. Similarly to lattice rotation, the distribution of shear strain increments is directly related to the position of yield surface in Mohr stress space. The symmetric yield locus gives us a symmetric displacement field and the asymmetric one is associated with asymmetric displacement field.

6.2.2. Lattice Rotation

Chen et al. [6] and Wang et al. [26] showed that plastic deformation under μLSP will cause rotation of crystallographic lattice. In Figure 6 we can see FEM simulation results of in-plane lattice rotation of Al of (110) and (1$\bar{1}$4) orientation. Green areas correspond to the unrotated lattice. Blue and red regions are related to the relative rotation of crystal axes [110]

and [1$\bar{1}$4] in respect to pre-treated position. It can be seen that in symmetric (110) orientation case two misoriented seen that lattice rotation is larger in double slip case regions and asymmetric yield loci. From Figure 6 it can also be seen that lattice rotation is larger in double slip case which is consistent with analytical prediction of plastic deformation derived in previous section.

6.3. Lattice rotation measurement via Electron Backscatter Diffraction (EBSD)

Lattice rotation of Al (110) and Al (1$\bar{1}$4) on the top surface and in cross-section is shown on the Figures 7 and 8, respectively. Rotation about shock line is anti-symmetric, the blue region corresponds to counterclockwise rotation, and the red region corresponds to clockwise rotation and green color indicates rotation free regions. Deformation is uniform along shock line, which shows plane strain condition is achieved by shocking single crystal along (110) direction. Deformation of (110) orientation is approximately symmetric, and wider than one in (1$\bar{1}$4) case, where blue region, is about 5 times smaller than red region. The magnitude of lattice rotation is largest between ±55 μm from the center of shock line and it is different for two cases: it is between ±4° for (110) and ±2° for (1$\bar{1}$4) orientation. Similar lattice rotation results, in terms of magnitude, can be observed in EBSD measurement of cross-section (Figure 8). Here in case of (110) orientation lattice rotates between ±2.35° which is almost twice as rotation of (1$\bar{1}$4) which is ±1.2°. Moreover, this result validates the assumption that double slip will cause greater rotation of lattice than single slip case, discussed in previous section. Therefore the analytical predictions are consistent with experimental measurements of lattice rotation. The difference in magnitude of rotation between experimental and numerical results is due the fact that in numerical simulation pressure loading is order of magnitude smaller than in experiment.

6.4. Stress Distribution

Analytical prediction of stress distribution by employment of anisotropic slip line theory in aluminum of (1$\bar{1}$4) orientation is discussed in detail in [26]. Although (110) orientation is more complex because of double slip, similar conclusions about stress distribution can be drawn for it [24]. Residual stress σ_{11} after unloading is shown at Figure 9. It can be seen that stress field is symmetric and residual stress near to the surface is mostly compressive.

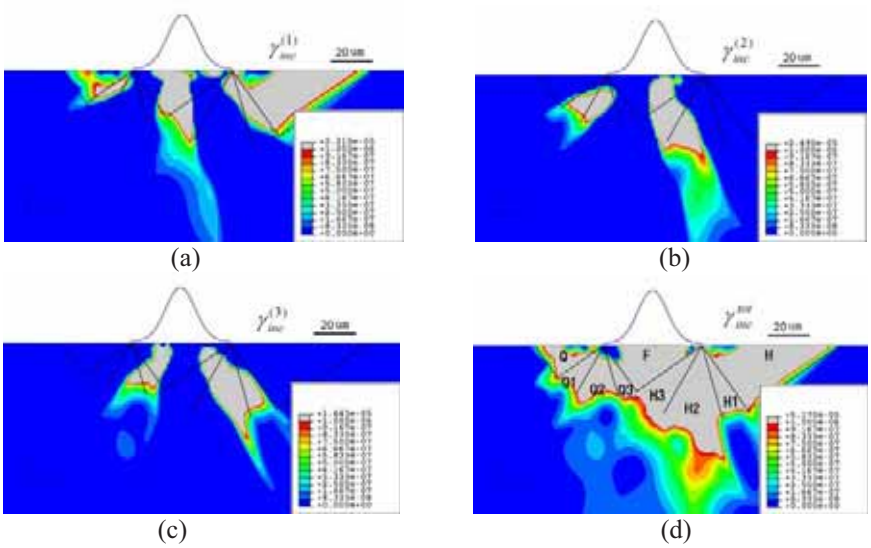

(a) (b) (c) (d)

Figure 5a: Shear strain increment in each slip system in the end of loading step for (1$\bar{1}$4) orientation: a) increment in slip system *i*; b) increment in slip system *iii*; c) increment in slip system *ii*; d) total shear strain increment

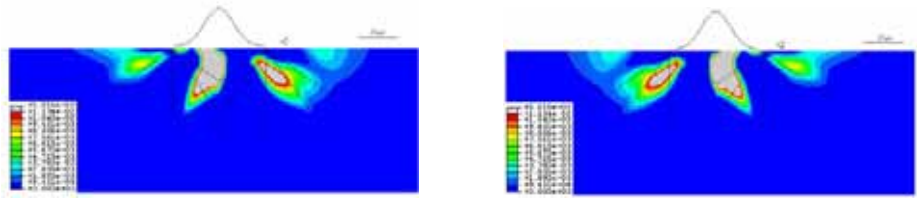

(a) (b)

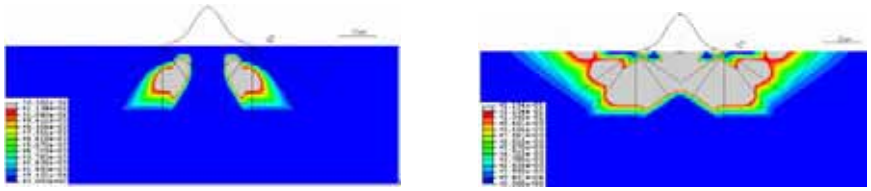

(c) (d)

Figure 5b: Shear strain increment in each slip system at the end of the loading step for [110] orientation a) increment in slip system i b) increment in slip system iii c) increment in slip system ii d) total shear strain increment

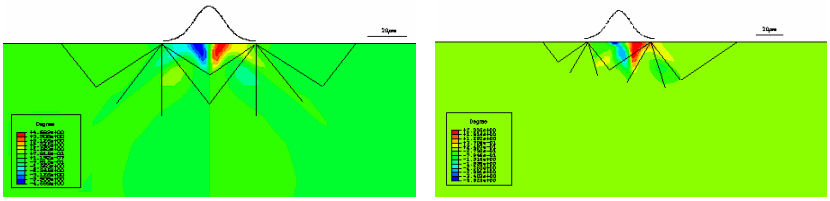

(a) (b)

Figure 6: Lattice deformation contour by FEM a) Orientation (110) b) Orientation (1$\bar{1}$4)

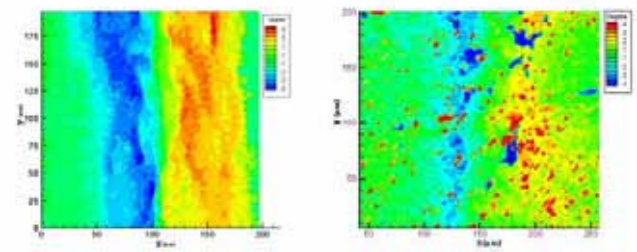

(a) (b)

Figure 7: Lattice rotation contour map on sample surface; a) Al (110) rotation b) Al (1$\bar{1}$4)

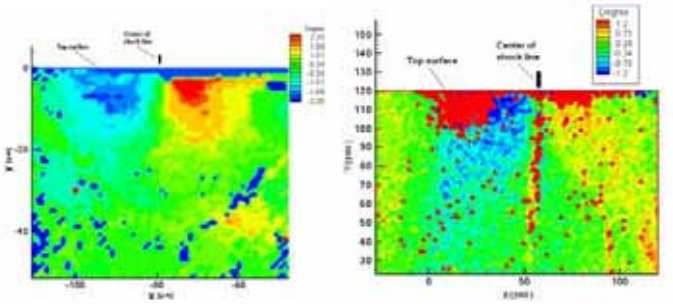

(a) (b)

Figure 8: Lattice rotation contour map on the (110) cross section. Positive rotation is counterclockwise about the z-axis

According to anisotropic slip line theory, within each sector stresses σ_{11} and σ_{22} are constant along α and β lines respectively. Stress changes rapidly between adjacent sectors. This is due to the fact that slip lines and slip normals represent places of stress discontinuity symmetric and residual stress near to the surface is mostly compressive. At the tips of the punch there are tensile regions which are explained in [26] by existence of region of the putative punch which causes positive σ_{11}. Furthermore, the ends of the punch represent singular points and therefore stress discontinuity region exists around them.

Using method proposed by Ungar [25] residual stresses were calculated from experimental results obtained via microdiffraction. Ungar's method assumes that deformed crystal is composed of cell walls and soft cell interiors. Cell walls are much harder than cell interiors and therefore the local flow stress is larger in cell walls in comparison to cell interiors. When pressure loading is applied to such a composite model, cell walls are under compression and interior experiences tensile stress. This can be observed in diffraction profile which is highly asymmetric close to the shock line and full width at compression and interior experiences tensile stress. This can be observed in diffraction profile which is highly asymmetric close to the shock line and full width at half at half maximum (FWHM) is increased as well. Thus

the asymmetric peak can be decomposed into two

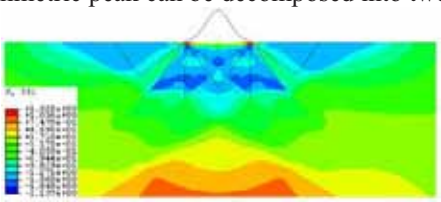

Figure 9: FEM Simulation of Residual Stress Distribution

symmetric peaks which belong to 'walls' and 'interiors', shifted to the left and right from undeformed peak, respectively. Measuring the relative difference in angle with respect to reference undistorted profile will lead to relative change of lattice spacing. This allows us to calculate $\Delta\sigma=(\Delta d/d)\cdot E$, for both cell walls and cell interiors. Residual stress in 3-3 direction is absolute value of difference between stresses in wall and interior. Assuming that stresses in 1-1 and 2-2 directions are equal they can be characterized as $\sigma_{11} = \sigma_{22} = -\sigma_{33}\nu$. The diffraction profile is measured along a line perpendicular to the shock line with 10 μm between each measurement. From Figure 10 it can be seen that residual stress is compressive within ±30 μm from center of the shock line and tensile in regions 30-60 μm away from line of shocking to the left and right.

Comparing figures 9 and 10 we see that there are some discrepancies between numerical and experimental results, caused by assumptions made while creating numerical model. Pressure loading in μLSP is one order

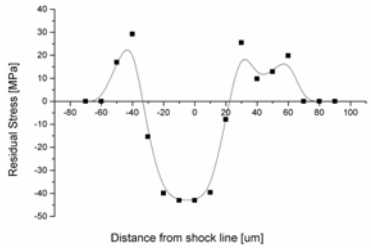

Figure 10: Residual stress measured via x-ray microdiffraction

of magnitude bigger than in model which causes difference in magnitude of residual stress. The numerical model does not take into account effect of strain hardening which leads to a stress affected zone is much greater in model that in experimental results. Loading in the model is static as opposed to the highly dynamic loading of μLSP. Due that fact, compressive residual stress near within ±30-60 μm range from center of shock line is not balanced with tensile stress in depth of material, as predicted by the model but rather near the surface on the left and right sides of the shocked line. Although it has limitations, numerical model can still give us a lot of information about the overall character of deformation process caused by μLSP. Despite discrepancies, trend of stress distribution matches experimental measurements, showing that stresses near to surface in region close to the shock line are mostly compressive which is beneficial for improvement of fatigue life of micro components.

7. Conclusion

Comparison between two different orientations of aluminum single crystal - one symmetric and one asymmetric - is presented in this paper. In this work, analytic, numerical and experimental investigations of two different orientations, (110) and $(1\bar{1}4)$ of aluminum single crystals are studied. Anisotropic slip line theory is employed for the construction of slip line fields for both orientations and compared with numerical results. In the case of double slip, shear stresses for each slip system have same sign, thus plastic deformation caused by each slip system adds to total deformation. This leads to the conclusion that deformation in symmetric orientation will be larger than in asymmetric case. A numerical model is established for more detailed investigation of μLSP process. It is validated through experiments. Experimental measurement of lattice rotation via EBSD in double slip case lattice rotation is twice as large as in single slip which validates analytic work. Residual stress is measured using x-ray microdiffraction and compared with numerical results. Future work will include effect of heterogeneity through study of grain boundary response to μLSP which will be achieved by examination of bicrystals.

8. Acknowledgment

This work is supported by National Science Foundation under grant DMI – 0500239. Dr. Jean Jordan Sweet of IBM Watson Research Center provided help with usage of X-ray microdiffraction equipment at the National Synchrotron Light Source at Brookhaven National Laboratory.
This work has used the shared experimental facilities that are supported primarily by the MRSEC Program of the National Science Foundation under Award Number DMR – 0213574 by the New York State Office if Science, Technology and Academic Research (NYSTAR). Dr. Paul van der Wilt assisted during EBSD measurements.

9. References

[1] Asaro, R.J. (1983) Micromechanics of crystals and polycrystals, Advances in Applied Mechanics 23, 1-115.
[2] Booker, J.R. & Davis, E.H., (1972) A general treatment of plastic anisotropy under conditions of plane strain, Journal of the Mechanics and Physics of Solids 20, 239-250.

[3] Crone, W.C., Shield, T.W., Creuziger, A. & Henneman, B., 2004) Orientation dependence of the plastic slip near notches in ductile FCC single crystals, Journal of the Mechanics and Physics of Solids 52, 85-112.
[4] Cullity, B.D. (1978) Elements of X-ray Diffraction, Addison-Weseley.
[5] Chen, H., Yao, Y.L. & Kysar, J.W. (2004) Spatialy resolved characterization of residual stress induced by micro scale laser shock peening, ASME, Transactions Journal of Manufacturing Science and Engineering 126, 226-235.
[6] Chen, H., Yao, Y.L. & Kysar, J.W. (2004) Characterization of plastic deformation induced by microscale laser shock peening, Journal of Applied Mechanics 71, 713-723.
[7] Clauer, A.H. & Holbrook, J.H. (1981) Effects of laser induced shock waves on metals, Shock waves and high strain phenomena in metals-concepts and applications, New York, Plenum, 675-702.
[8] Clauer, A.H. & Lahrman, D.F. (2001) Laser Shock processing as a surface enhancement process, Key Engineering Materials 197, 121-142.
[9] Fabbro, R., Fournier, J., Ballard, P., Devaux, D. &
[10] Virmont, J. (1990) Physical study of laser-produced plasma in confined geometry, Journal of Applied Physics 68, No. 2, 775-784.
[11] Fox, J.A. (1974) Effect of Water and Paint Coatings on Laser-Irradiated Targets, Applied Physics Letters 24, 461-464.
[12] Hertzberg, R.W. (1995) Deformation and Fracture Mechanics of Engineering, John Wiley and Sons.
[13] Hammersley, G., Hackel, L.A. & Harris, F. (2000) Surface prestressing to improve fatigue strength of components by laser shot peening, Optics and Lasers in Engineering 34, 327-337.
[14] Hill, R., (1950) The Mathematical Theory of Plasticity, Claredon Press,
[15] Huang, Y. (1991) A User-material subroutine incorporating single crystal plasticity in the ABAQUS finite element program, Mech. Report, 178, Division of Applied Sciences, Harvard University, Cambridge, MA.
[16] Katchanov, L.M. (1971) Foundations of The Theory of Plasticity, North-Holland.
[17] Kysar, J. (1997) Addendum to a user-material subroutine incorporating single crystal plasticity in the ABAQUS finite element program, Mech. Report, 178, Division of Applied Sciences, Harvard University, Cambridge, MA.
[18] Kysar, J.W. & Briant, C.L. (2002) Crack tip deformation fields in ductile single crystals, Acta Materialia 50, 2367-2380.
[19] Kysar, J.W., Gan, Y.X. & Mendez-Arzuza, G. (2005) Cylindrical void in a rigid-ideally plastic single crystal. Part I: anisotropic slip line theory solution for face-centered cubic crystals, International Journal of Plasticity 21, 1481-1520.
[20] Noyan, I.C. & Cohen, J.B. (1986) Residual Stress, Springer-Verlag New York, Inc.
[21] Hencky, H. (1923) Über einige statisch bestimmte fälle des gleichgewichts in plastischen körpern, Z. Angew. Math. Mech. 3, 241–251 (German).
[22] Prandtl, L. (1923) Anwendungsbeispiele zu einem henckyschen salt über das plastische gleichgewicht, Zeitschr. Angew. Math. Mech. 3, 401-406.
[23] Rice, J.R. (1973) Plane strain slip line theory for anisotropic rigid/plastic materials, Journal of the Mechanics and Physics of Solids 21, 63 -74.
[24] Rice, J.R. (1987) Tensile crack tip fields in elastic-ideally plastic crystals, Mechanics of Materials 6, 317-335.
[25] Ungar, T., Mughrabi, H., Roennpagel, D. & Wilkens, M. (1984) X-ray line-broadening study of the dislocation cell structure in deformed [001]-oriented copper single crystals, Acta Metallurgica 32(3), 332-342.
[26] Wang, Y., Kysar, J.W. & Yao, Y.L. (2005) Analytical solution of anisotropic plastic deformation induced by micro-scale laser shock peening, Submitted.
[27] Zhang, W. & Yao, Y.L. (2002) Microscale laser shock processing of metallic components, Journal of Solar Energy Engineering, Transactions of the ASME, 124, 369-378.

Sinisa Vukelic is a Ph.D candidate at Columbia University. He received his BS from University of Belgrade (2004), and MS from Columbia University (2005). His research interests are laser shock peening and laser peen forming.

Youneng Wang is a Ph.D candidate at Columbia University. He received his BS and MS from University of Science and Technology of China and University of Michigan, respectively. His research interests are laser shock peening and laser micromachining.

Jeffrey W. Kysar is an Associate professor at Columbia University. He received his Ph.D. from Harvard University and his research interests are micromechanics of facture in ductile materials, and multi-scale experiments and modeling of fracture.

Y. Lawrence Yao is a Professor at Columbia University. He received his Ph.D. from the University of Wisconsin-Madison in 1988. He is interested in multidisciplinary research in manufacturing and design, nontraditional manufacturing processes and laser materials processing. He serves on the Board of Directors of LIA.